energies

MDPI

Article

Preliminary Development of a Free Piston Expander–Linear Generator for Small-Scale Organic Rankine Cycle (ORC) Waste Heat Recovery System

Gaosheng Li [1,2], Hongguang Zhang [1,2,*], Fubin Yang [1,2], Songsong Song [1,2], Ying Chang [1,2], Fei Yu [1,2], Jingfu Wang [1,2] and Baofeng Yao [1,2]

[1] College of Environmental and Energy Engineering, Beijing University of Technology, Pingleyuan No. 100, Beijing 100124, China; gao.sheng2005@163.com (G.L.); yangfubinnuc@163.com (F.Y.); qihesong@126.com (S.S.); changying16688@126.com (Y.C.); yufei19910726@gmail.com (F.Y.); jfwang@bjut.edu.cn (J.W.); yaobf@bjut.edu.cn (B.Y.)

[2] Collaborative Innovation Center of Electric Vehicles in Beijing, Pingleyuan No. 100, Beijing 100124, China

* Correspondence: zhanghongguang@bjut.edu.cn; Tel.: +86-10-6739-2469

Academic Editor: K. T. Chau

Received: 24 January 2016; Accepted: 14 April 2016; Published: 20 April 2016

Abstract: A novel free piston expander-linear generator (FPE-LG) integrated unit was proposed to recover waste heat efficiently from vehicle engine. This integrated unit can be used in a small-scale Organic Rankine Cycle (ORC) system and can directly convert the thermodynamic energy of working fluid into electric energy. The conceptual design of the free piston expander (FPE) was introduced and discussed. A cam plate and the corresponding valve train were used to control the inlet and outlet valve timing of the FPE. The working principle of the FPE-LG was proven to be feasible using an air test rig. The indicated efficiency of the FPE was obtained from the p–V indicator diagram. The dynamic characteristics of the in-cylinder flow field during the intake and exhaust processes of the FPE were analyzed based on Fluent software and 3D numerical simulation models using a computation fluid dynamics method. Results show that the indicated efficiency of the FPE can reach 66.2% and the maximal electric power output of the FPE-LG can reach 22.7 W when the working frequency is 3 Hz and intake pressure is 0.2 MPa. Two large-scale vortices are formed during the intake process because of the non-uniform distribution of velocity and pressure. The vortex flow will convert pressure energy and kinetic energy into thermodynamic energy for the working fluid, which weakens the power capacity of the working fluid.

Keywords: free piston expander (FPE); conceptual design; cam plate; dynamic characteristics; 3D numerical simulation

1. Introduction

The internal combustion (IC) engine, which is the power system of an automobile, consumes a tremendous amount of energy. As energy shortages are continuously worsening, the energy-efficient utilization of IC engines has attracted increasing attention from researchers for a long time now. Only one-third of the energy from fuel combustion is utilized effectively in IC engines, whereas the rest is wasted in various forms of cooling, exhaust, and mechanical losses; exhaust energy accounts for the largest proportion of wasted energy in IC engines [1–4]. Therefore, recovering exhaust energy is an effective means to save vehicle energy. In the case of waste heat recovery (WHR), the Organic Rankine Cycle (ORC) system is an effective technical solution and a promising means for industrialization of energy savings [5–7]. To date, research on ORC applications has mostly focused on large-scale heat sources, such as solar energy, geothermal energy, and industrial waste heat, *etc.* [8–12]. The lack of a suitable expander has caused difficulties in building corresponding ORC systems for recovering

small-scale waste heat, such as vehicle exhaust energy, *etc.* At present, developing an ideal small-scale expander or power output system that can convert waste heat into mechanical energy or electric energy to recover exhaust energy from vehicle IC engines is a crucial objective of ORC system research [13–15].

An expander is a key component in an ORC system. Compared with a centrifugal expander, a positive displacement expander is characterized by low flow rate, large expansion ratio, and low rotational speed [15–17]. A positive displacement expander should therefore be more suitable for a small-scale ORC system [18,19]. However, low cost and low rotational speed scroll expanders are frequently used in 0.1–2 kW experimental systems, whereas their performance in situations involving higher power has not been verified yet [20–22]. A piston expander has higher thermal efficiency for small steam flow rate conditions and a good power output/size ratio. This type of expander is generally built or renovated based on existing commercial IC engines. If the pressure ratio on the expander is high, then piston expanders are suitable. Moreover, these expanders are more robust than scroll expanders. Gao *et al.* [23] constructed a mathematical model to evaluate the performance of a Rankine cycle system with a reciprocating piston expander and conducted a preliminary experiment. The results showed that the introducing a heat recovery system could increase engine power output by 12% when a diesel engine was operated at 80 kW/2590 rpm. Glavatskaya *et al.* [24] investigated the performance of a reciprocating expander for an automotive WHR application. The results showed that a maximum power output of 7 kW could be obtained at a high operating point, and the isentropic efficiency of the reciprocating expander varied from 55% to 70%. Chiong *et al.* [25] presented a concept for a new piston expander utilizing a nozzle as part of a secondary steam cycle to recover exhaust energy. Through simulation, the nozzle piston expander was found to increase the output power from a minimum of 0.73 kW to a maximum of 4.75 kW. The aforementioned survey of Rankine cycle systems applied to passenger vehicles indicates that the piston expander is a promising technology for WHR applications compared with other types of expander. This technology is innovative in the automotive industry [23–26]. However, a comparatively large weight and a complicated structure restrict the extensive application of piston expanders in small-scale vehicle ORC systems.

To overcome the aforementioned shortcomings of piston expanders, the concept of a free piston expander (FPE), which is characterized by cancelling the crank-link mechanism, has been presented [27–32]. Zhang *et al.* [27] developed a FPE that could be used in the transcritical CO_2 refrigeration cycle to replace the throttling valve. An expansion machine was integrated into a compressor in this device, and thus, the crankshaft became unnecessary. Moreover, a slide valve was designed to replace the traditional inlet/outlet valves to control the charge/discharge process. The design efficiencies of the expander and the compressor were assumed to be 60% and 70%, respectively; the experimental studies using p–V diagrams showed that device isentropic efficiency could reach 62%. Han *et al.* [28,29] constructed a simulation model and a test bench for a similar Rankine cycle WHR system using a FPE. Subsequently, a preliminary experiment was conducted. The power output of the free piston mechanism was eventually consumed through hydraulic buffers and reached 2.08 kJ, whereas piston displacement was 52 mm when the evaporator outlet pressure of the working fluid was 0.7 MPa. Weiss *et al.* [30] designed a FPE to produce power using a low-temperature energy source, and the FPE model was studied under various conditions. The results showed that decreasing piston mass reduced piston stroke length, but increased operation frequency and power output. Power output and energy recovery efficiency reached 25.6 mW and 80%–90%, respectively. Champagne *et al.* [31] conducted a preliminary experimental analysis of a small-scale FPE. The results showed that lubricants significantly affected the seal and leakage of a FPE. A thick lubricant seal was better in static configurations than in dynamic testing. Nickl *et al.* [32] developed a free piston compressor–expander unit with three expansion stages, and the isentropic efficiency of this device could reach 70% during the tests.

In the present research, a novel free piston expander-linear generator (FPE-LG) is proposed based on previous design experiences and the considerable literature on FPE prototypes mentioned earlier [27–32]. Compared with the ORC power generation system that uses a conventional expander,

an ORC power generation system based on FPE-LG exhibits certain advantages such as compact structure, operation flexibility, and effective power output under the action of a two-phase flow in a partial load condition [30,31]. In addition, FPE-LG is more suitable for ethanol and the water Rankine cycle because of its large expansion ratio. A small-scale ORC system with FPE-LG can transform waste heat from IC engine exhaust into electricity and subsequently supply power to the powertrain or auxiliary load of the vehicle.

In this research, a novel FPE-LG was developed, and several preliminary experiments were performed using an air test rig. For the intake and exhaust processes of the FPE, the dynamic characteristics of the in-cylinder flow field were analyzed using a computational fluid dynamics (CFD) method and Fluent software.

2. Experimental Setup and Procedure

2.1. Working Principle and Function of the Free Piston Expander-Linear Generator

The FPE-LG mainly consists of two FPEs and a linear generator (LG). The LG mover is connected to the piston rods through flexible joints. This LG mover executes a reciprocating linear movement because of the gas pressure difference between the top of the two free pistons. The kinetic energy of the mover can be converted into electric energy by the LG. The valve train of the FPE is driven by a servo motor. In a formal engine application, the operation power of the servo motor will be provided by the engine-generated electrical output. When the FPE is in an intake-expansion stroke, the piston moves from top dead center (TDC) to bottom dead center (BDC). The working fluid flows first into the cylinder (*i.e.*, intake process, the inlet valve is open and the outlet valve is closed), and then expands in the cylinder (*i.e.*, expansion process, the inlet valve and outlet valves are both closed). When the FPE is in an exhaust stroke, the piston moves from BDC to TDC, and then the working fluid flows out of the cylinder (*i.e.*, exhaust process, the inlet valve is closed and the outlet valve is open). When FPE A is in intake-expansion stroke, FPE B is in exhaust stroke, and *vice versa*. The LG is the sole energy output device of the FPE-LG, and thus, selecting an appropriate LG in the conceptual design stage is crucial.

For the same geometry size, a flat permanent magnet LG is easily constructed and exhibits good excitation; meanwhile, its output voltage, current effective value, efficiency, and specific power are slightly higher than those of the tubular permanent magnet LG with the same load [33,34]. Therefore, a flat permanent magnet LG is selected to match with the FPEs in this research. The manufactured FPE-LG prototype is shown in Figure 1.

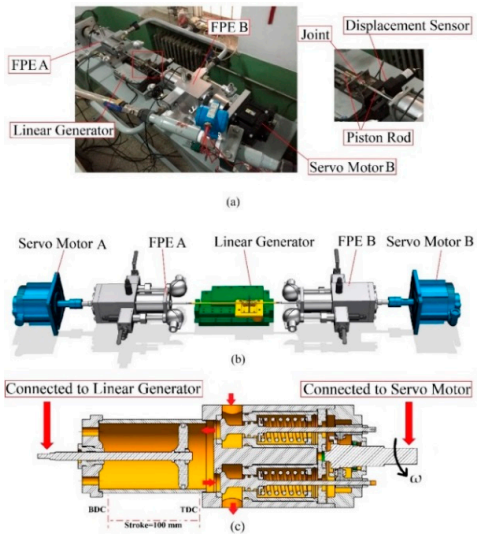

Figure 1. Prototype and 3D model of the free piston expander-linear generator (FPE-LG): (**a**) FPE-LG prototype; (**b**) 3D model of the FPE-LG; (**c**) Cross-sectional view of the free piston expander (FPE).

Figure 2 presents the schematic diagram of a small-scale ORC system using the FPE-LG for recovering exhaust energy from vehicle engines. The key components are the evaporator, the FPE-LG, the condenser, the working fluid tank, and the working fluid pump. During the ORC WHR system operation process, the organic working fluid is pressurized by the pump and absorbs heat from low-medium grade waste heat source (*i.e.*, engine exhaust) in the evaporator. Then, this fluid turns into high pressure and high temperature vapor and flows into the FPE-LG. This unit can convert the thermodynamic energy of the working fluid into electric energy (electric power can be consumed by the load resistance). After expanding in the FPE, the low pressure and low temperature vapor flows into the condenser. Then, this vapor turns into liquid and flows into the tank. The overall operation performance of the FPE-LG changes with working conditions, such as evaporation pressure, condensation pressure, and load resistance, *etc.* As shown in Figure 2, on the one hand, FPE converts the energy stored in the working fluid that enters the FPE into the kinetic energy of the free piston. The piston-mover group is driven to perform an oscillating linear movement according to the energy conservation law (various losses are neglected). On the other hand, the electromotive force is in proportion to the motion speed of the piston-mover group according to Faraday's law of electromagnetic induction. Hence, a reasonable conceptual design of the FPE is beneficial for reducing losses in the energy conversion process. Such a design also significantly influences the overall energy conversion efficiency of the FPE-LG. We primarily focus on the FPE in this research because of the aforementioned reasons.

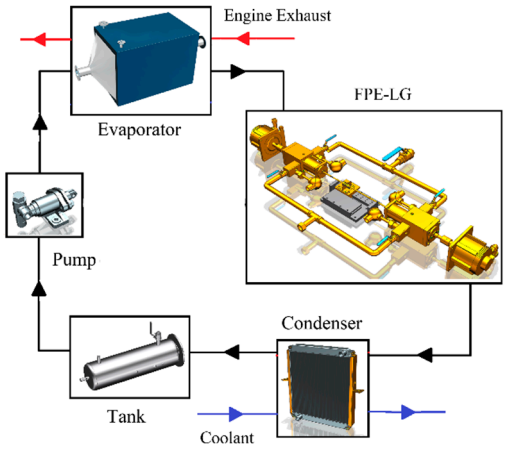

Figure 2. Schematic diagram of small-scale Organic Rankine Cycle (ORC) system using FPE-LG.

2.2. Conceptual Design of the Free Piston Expander

2.2.1. Configuration and Main Parameters

According to a large number of measured experimental data, the restricted conditions for the FPE design are listed as follows:

(1) Intake temperature of the working fluid is 300–350 K;
(2) Intake pressure of the working fluid is 0.8–1 MPa;
(3) Maximal expansion ratio of the FPE is 9;
(4) Intake volume flow rate of the working fluid is 10–20 m^3/h;
(5) Exhaust back pressure is 0.11–0.13 MPa.

Figure 3 shows the configuration diagram of the manufactured FPE. The main components include: valve train, piston, piston rod, cylinder cover, cylinder block, cylinder head, and rear cover, *etc.* The inlet and outlet valves are normally closed because of the precompression force of the valve spring. According to the precompression and stiffness of the valve spring as well as the maximal working

frequency (8 Hz) of the FPE, the torque output of the servo motor should be higher than 10 N· m to open the inlet (or outlet) valve reliably during the intake process (or exhaust process). Thus, the specific servo motor (operating voltage is 200 V, rated torque output is 15 N· m) is used to drive the valve train. The servo motor is connected with the drive shaft of the valve train through a flexible shaft coupling. The piston rod of the FPE is connected with the mover of the LG through flexible joints. The specific design objectives of prototype performance are determined by considering the requirements for related projects and current experimental research status, and are listed as follows: output power of the FPE-LG is 1 kW and its maximal working frequency is 8 Hz. Hence, the main structure parameters of the FPE-LG prototype were determined according to the design method introduced in [35], as listed in Table 1:

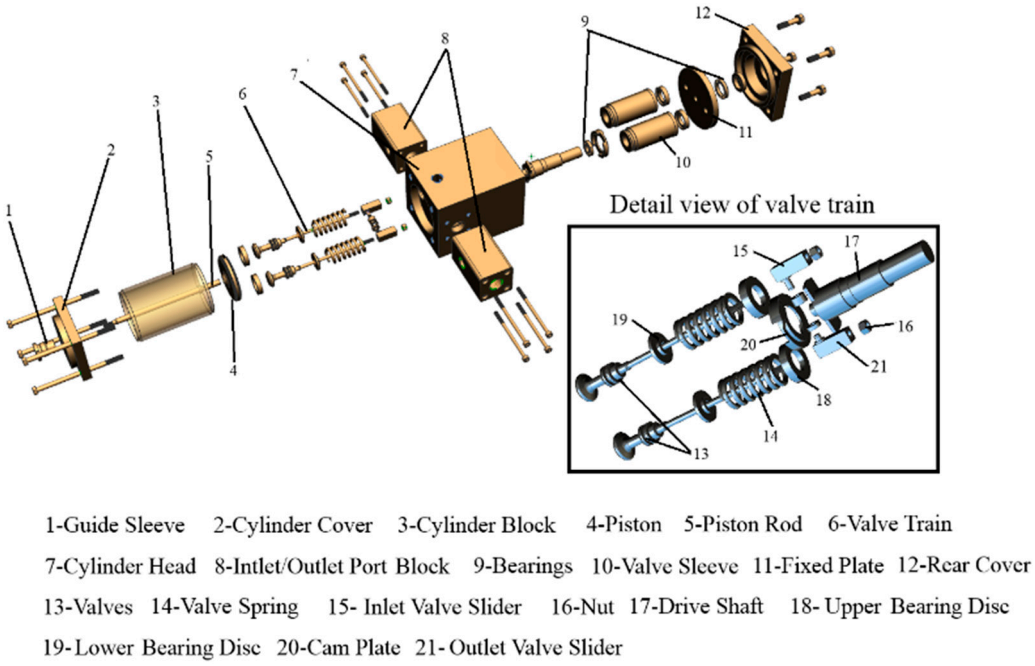

Figure 3. Exploded view of the FPE configuration (small fasteners are omitted for clarity).

Table 1. The main construction parameters of FPE.

Items	Parameters	Units
Cylinder diameter	80	mm
Working frequency	1–8	Hz
Maximal piston stroke length	100	mm
Intake duration	0–90	degree
Exhaust duration	180–360	degree
Piston rod diameter	10	mm
Inlet port diameter	22	mm
Outlet port diameter	25	mm
Relative clearance factor	1/18	-

As mentioned earlier, piston expanders have several drawbacks that will restrict their extensive application in small-scale ORC systems. In comparison, the FPE-LG is an electrically and mechanically integrated unit that does not require a crankshaft. The output power of a single reciprocating piston expander may be larger than that of the FPE-LG. In its final form, however, the FPE-LG will be designed to be modular, and thus, additional installation space is unnecessary. The number of these units can be adjusted flexibly according to the output power requirement for small-scale vehicle ORC systems. In addition, this FPE-LG is the first generation prototype. We will increase the working frequency

gradually in a further study based on the preliminary results of motion characteristic in the current research. The final design objective of the working frequency ranges from 30 Hz to 40 Hz.

2.2.2. Energy Loss Mechanisms

The FPE-LG is an ideal energy conversion device for a small-scale ORC WHR system because of its characteristics of less mechanical loss and compact configuration. Compared with the ideal working process of the FPE, several primary loss mechanisms are involved in the actual operation process of the FPE. Such mechanisms can be summarized as follows:

(1) Incomplete expansion. During the expansion process, the expansion of the working fluid in the cylinder is incomplete because of the limitation in actual piston stroke and valve timing. In-cylinder pressure is higher than exhaust back pressure at the end of expansion process;
(2) Heat transfer. The working process of the FPE is not adiabatic because of the temperature difference between the FPE cylinder (or working fluid) and the ambient environment. Thus, heat exchange occurs between the FPE cylinder (or working fluid) and the ambient environment;
(3) Flow loss during intake and exhaust processes. The inlet and outlet valves are used to control inlet and outlet valve timing, respectively; hence, flow loss occurs in the actual intake and exhaust processes;
(4) Mechanical friction. The primary mechanical friction occurs in the following contact segments: piston and cylinder wall, piston rod and guide sleeve, drive shaft and bearing/cover, cam plate and valve slider, *etc.* A wear-resistant material with high strength (e.g., aluminum alloy and aluminum bronze) is used in designing the FPE process to reduce wear and improve the fatigue life of relevant components;
(5) Leakage. When the cylinder is full of working fluid, there exists more or less leakage in the gap between the piston and cylinder wall.

2.2.3. Lubrication and Sealing

The maximal in-cylinder pressure of the FPE is limited to 0.8–1 MPa. The working fluid may leak through various gaps during the FPE operation process, including the gaps between the piston and cylinder wall, between the cylinder block and cylinder cover, and between the cylinder block and cylinder head. Hence, ring grooves on both ends of the cylinder are designed to install sealing rings constituted by polytetrafluoroethylene (PTFE). The piston ring is also constituted by PTFE. PTFE can reduce the friction between the sealing ring and the corresponding contact segments as well as perform a sealing function because of its self-lubricating property. Mechanical wear mainly occurs in the valve train and in the piston-mover group during the operation process of the FPE. The lubricating oil is injected through the oil holes processed on the rear cover and into the enclosed chamber between the rear cover and the cylinder head, where the cam plate of the valve train and some moving parts are located. Therefore, the corresponding contact segments can be lubricated through splash lubrication when the cam plate rotates during the operation process of the FPE. The piston rod performs a rapid reciprocating movement when passing through the guide sleeve. Meanwhile, installation errors exist in the alignment, which can lead to friction and wear. Hence, aluminum bronze is selected as the constituent material of the guide sleeve. Heat treatment technology is also adopted to satisfy the requirements of strength and reliability. Meanwhile, lubricating grease is inserted into the inner hole of the guide sleeve. This design is beneficial for reducing friction and wear.

2.2.4. Valve Train

The valve train signifcantly influences the stable operation of the FPE and flow loss during its intake and exhaust processes [36,37]. Two kinds of valve trains can be selected for the FPE, namely, mechanical control valve manner and electromagnetic control valve manner. The former is used in this research after considering the manufacturing cost and working frequency of the FPE [37]. As shown in

Figure 4, a mechanical control valve train using a rotational cam plate has been developed. The specific servo motor (operating voltage is 200 V, rated torque output is 15 N· m) is utilized to drive the valve train. The output end of the servo motor is connected to the drive shaft of the valve train through a flexible shaft coupling.

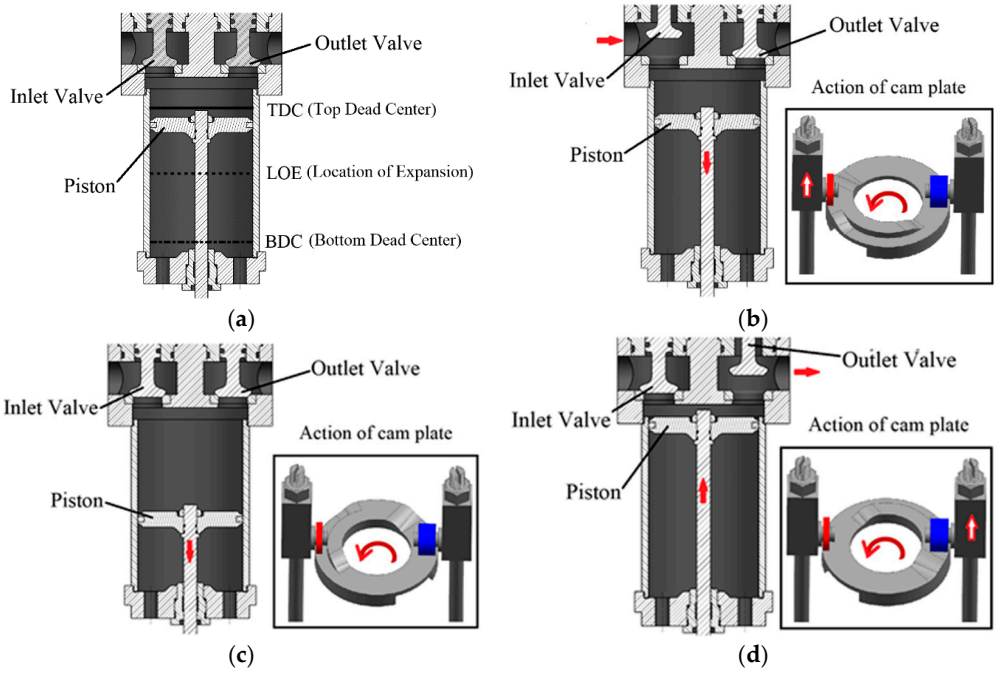

Figure 4. Working process of FPE and corresponding behaviors of the valve train: (**a**) initial position; (**b**) intake process; (**c**) expansion process; (**d**) exhaust process.

Figure 4 illustrates the working process of the FPE and the corresponding behavior of the valve train. The entire working process (cycle) of the FPE includes two strokes: intake-expansion and exhaust. An intake-expansion stroke includes the intake and expansion processes, whereas an exhaust stroke includes only the exhaust process. For the initial position, as shown in Figure 4a, under the action of return force of the valve spring, the inlet and outlet valves are both closed, and the piston-mover group is located at TDC. During the intake process, as shown in Figure 4b, the cam plate axially lifts up the inlet valve slider and then opens the inlet valve by overcoming the return force of the valve spring. The working fluid flows into the cylinder through the inlet port and the inlet valve; the piston-mover group moves from TDC to BDC. During the expansion process, as shown in Figure 4c, the inlet and outlet valves are both closed under the action of the return force of the valve spring. The working fluid expands in the cylinder and pushes the piston-mover group to BDC. During the exhaust process, as shown in Figure 4d, the cam plate axially lifts up the outlet valve slider and then opens the outlet valve by overcoming the return force of the valve spring. The piston-mover group moves from BDC to TDC, and working fluid flows out of the cylinder and through the outlet port and the outlet valve.

2.3. Air Test Rig of the Free Piston Expander-Linear Generator

As the manufactured FPE-LG is a novel energy conversion device for a small-scale ORC WHR system, the air test rig is first established to verify the working principle and feasibility of the FPE-LG. According to the test results, FPE-LG may be subsequently integrated into the ORC WHR system after implementing several improvements (or adjustments) to the FPE-LG. Figure 5 shows the air test rig for the FPE–LG. This rig mainly includes an air compressor, a compressed air tank, the FPE-LG, an electric load, different kinds of sensors, data acquisition system, *etc.* Compressed air is used as the working fluid in the experiment because of two main reasons [38]. First, supplying and consuming compressed

air in the experiment are convenient. Moreover, the properties of compressed air are close to those of ideal gas, and compressed air does not exhibit any phase change in the experiment. Second, although the properties of compressed air and the vapor state of an organic working fluid are significantly different, this difference only has a slight influence on the test results of the feasibility of the FPE-LG as well as the valve train.

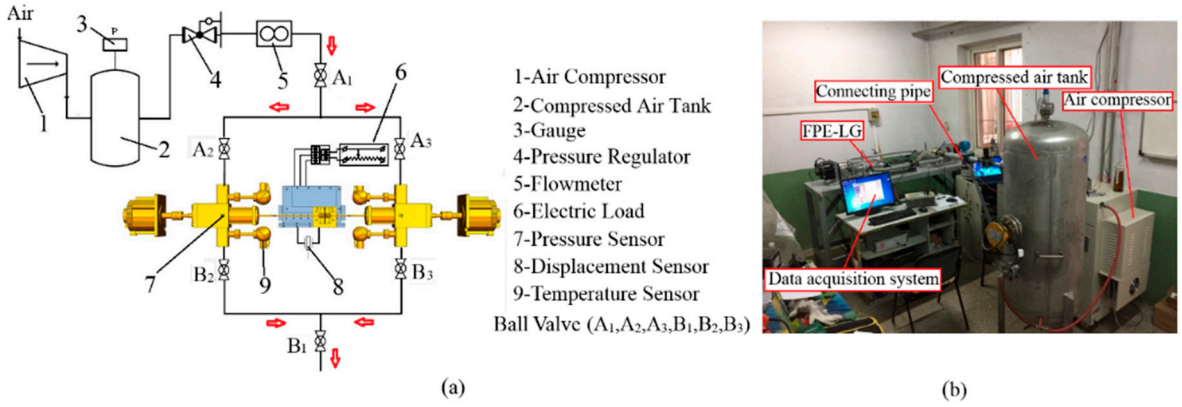

Figure 5. Air test rig of the FPE-LG: (**a**) the schematic diagram of experimental system; (**b**) the picture of experimental system.

2.4. Experimental Procedure

The flow rate of the working fluid can be regulated by adjusting the opening degree of the ball valves. The temperature sensors and pressure sensors are installed into the two FPEs. A displacement sensor is also installed and used to indicate the displacement variation of the piston-mover group during the working process of the FPE-LG. A phase difference of 180° is observed between the cam plates of the two FPEs under the control of the two servo motors, which ensures that the working process and the piston stroke of the two FPEs are coordinated. A flowmeter is installed to measure the total flow rate of the working fluid for the two FPEs. The electrical output of the LG can be converted to direct current electricity by using the three-phase bridge rectifier and the smoothing capacitor. The main test instrumentations of the experimental procedure are listed in Table 2.

Table 2. The main test instrumentations of the experimental procedure.

Items	Type	Technical parameter
Pressure sensor	TCT–1201	Power supply is 24 V, range is 0–1.5 MPa, accuracy is ±0.2%
Temperature sensor	WZ/P–DK	Power supply is 24 V, range is −20–100 °C, accuracy is ±0.5%
Draw wire position transducer	TWLB	Power supply is 24 V, range is 0–400 mm, accuracy is 0.5%
Flow rate measurement	Volumetric turbo flow meter	Range is 5–42 m^3/h, temperature range is −50–180 °C, accuracy is ±1.5%

3. Results and Discussion

3.1. Three-Dimensional Numerical Simulation of the Free Piston Expander

To explore the dynamic characteristics of the in-cylinder flow field during the intake and exhaust processes of the FPE, three-dimensional (3D) numerical simulation of the FPE is implemented by using Fluent V14.0 based on the control volume methodology of the combined dynamic meshing technique [39].

3.1.1. Grid Generation

The 3D grid is built using Gambit 6.0 because of the complex geometric model established in Catia V5R21. The mesh model of the FPE is shown in Figure 6. The computational grid of the FPE consists of 2,031,293 elements and 3,937,918 nodes. The internal calculation fluid region of the FPE is composed of three sub-fluid regions, which are separated by the inlet and outlet valves. The unstructured tetrahedral grid is used to mesh the inlet and outlet fluid regions (fluid regions B and C, respectively, in Figure 6) with the smallest unit size of 0.2 mm. The submap structured hexahedral mesh with the minimum unit size of 0.4 mm is adapted to the in-cylinder fluid region (fluid region A in Figure 6) because of its regular cylindrical shape. The valves and the piston are meshed by the unstructured tetrahedral grid with the smallest unit sizes of 0.2 mm and 0.4 mm, respectively. The gap between the valve and the valve seat is 0.1 mm. The grid of the sub-fluid regions near the valves is refined with the minimum unit size of 0.1 mm after considering the dramatic change in the flow field. Interface technology is applied to ensure the variable interpolation and delivery of the overlapping segments in different fluid regions.

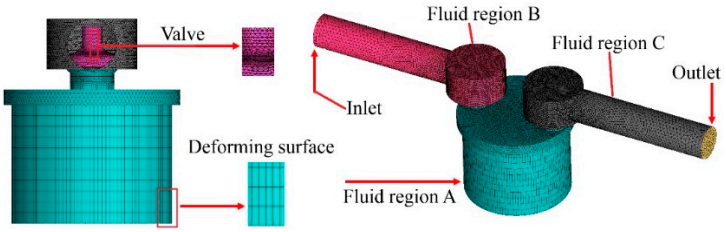

Figure 6. Computational domains of the FPE.

3.1.2. Boundary Conditions and Dynamic Mesh

The numerical simulation of unsteady flow in the FPE is implemented using the renormalization group-based k–ε turbulence model in Fluent V14.0 [39]. The thermodynamic properties of the working fluid can be determined using REFPROP software developed by the National Institute of Standards and Technology (NIST). The calculation difficulties are attributed to the grid varying constantly as a result of the movement of the valves and the piston during the working process of the FPE. Thus, dynamic mesh definition is necessary for the aforementioned moving components. The motion characteristics of the valves can be converted into the equivalent relationship between valve displacement and elapsed time according to cam plate profile and working frequency. Consequently, a control program is compiled to regulate the dynamic grid for the valves. This control program can be derived from the experimental results of the piston movement and the force analysis results during the working process of the FPE through MATLAB Simulink.

The working conditions of the FPE for the numerical simulation are set as follows: intake pressure is 0.2 MPa, intake temperature is 300 K, and working frequency of the FPE-LG is 3 Hz. Air is used as working fluid in the CFD simulation model. The property parameters of air are obtained from the average temperature and average pressure of the inlet and outlet of the FPE using NIST-REFPROP. The outlet boundary condition is set to atmospheric pressure, whereas heat transfer between the cylinder wall and the ambient environment is disregarded. Simultaneously, the average time step, which can be adjusted to suit the moving situations of the valves and the piston, is set to 1×10^{-4} s. In this manner, negative volume will not be generated when the dynamic mesh updates the position. Residual, pressure, and turbulence intensity variations can be monitored in real time to observe the convergence and results of the numerical calculation.

3.1.3. Unsteady Flow Behavior during the Intake and Exhaust Processes

Figure 7 shows the complex vortex flow in the cylinder when the rotational angle of the cam plate is 75° after the beginning of the curved surface for lifting the inlet valve during the intake

process. At the beginning of the intake process, the working fluid with high pressure is injected into the cylinder through the narrow flow area between the inlet valve and the inlet valve seat. Thus, given the small opening degree of the inlet valve, the Laval nozzle effect may occur in the narrow flow area. Simultaneously, the narrow flow area between the inlet valve and the inlet valve seat exhibits evident pressure drop, throttling loss, and turbulence intensity. A local high-pressure zone A is formed in the half cavity around the inlet valve because of the inlet port wall. Simultaneously, gas flows along the valve axes with a tremendously high velocity in the cylinder, which results in low pressure in the gas flow core region. Thus, a local high-pressure zone B is formed in the small cylindrical cavity between the cylinder head and cylinder wall (below the inlet valve). The mainstream continues flowing along the tangential direction of the cylinder wall and the piston top. A local high-pressure zone C is formed in a short channel (between the outlet valve and the cylinder wall) below the outlet valve. Subsequently, gas flows toward the main intake stream along the tangential direction of the cylinder head surface because of the pressure gradient between the core region of the mainstream and zone C. Gas flow is merged into the newly injected intake flow because of viscous force. Thecore region of the vortices is another high-pressure zone (marked with the letter D in Figure 7). Two large-scale vortices V_1 and V_2 are formed during the intake process.

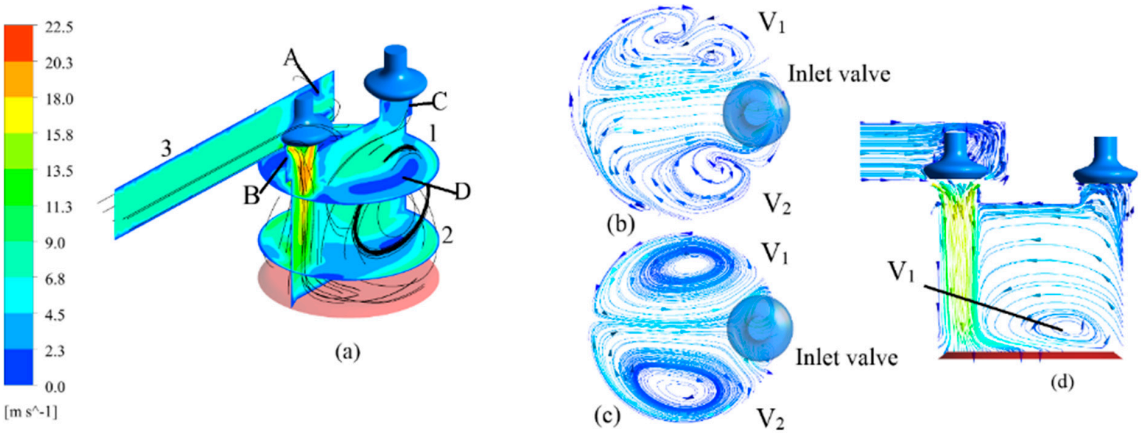

Figure 7. Vortex flow in cylinder during the intake process: (**a**) Main view; (**b**) View 1: cross-section vertical to the inlet valve axis, 10 mm below the inlet valve; (**c**) View 2: cross-section vertical to the inlet valve axis, 50 mm below the inlet valve; (**d**) View 3: longitudinal-section along the valve axes.

Figure 8 shows the gas velocity distribution and streamlines during the intake process at different rotational angles of the cam plate after the beginning of the curved surface for lifting up the inlet valve (ranges from 2° to 88°). When the opening degree of the inlet valve is relatively small, a large flow resistance occurs, which results in the low pressure in the cylinder. Hence, gas flow around the inlet valve head is injected into the cylinder along the tangential direction of the inlet valve head through the narrow flow area between the inlet valve and the inlet valve seat because of the considerable pressure difference. Moreover, gas flow is separated into two branches after it comes in contact with the piston top and subsequently compresses the original gas in the cylinder respectively. Consequently, the distribution of velocity and pressure becomes non-uniform. As shown in Figure 8a,b, no obvious large-scale vortex is formed in the cylinder because of the relatively small cylinder volume. Subsequently, the volume of intake flow gradually increases with piston movement. Two large-scale vortices (V_1 and V_2) are formed in the cylinder, as shown in Figure 8c, because of the restriction imposed by the solid wall (which is constructed by the cylinder wall, piston top, and cylinder head surface). Vortices V_1 and V_2 are gradually enhanced with the increase in inlet valve opening degree because the volume of intake flow rapidly increases with the increase in the flow area between the inlet valve and the inlet valve seat, as shown in Figure 8d. When the inlet valve is fully opened, the gas continues flowing into the cylinder. However, the pressure difference between the inlet port and the

cylinder becomes small. At this point, the distribution of gas velocity and pressure generally becomes relatively uniform in the cylinder, and two stable vortices are formed in the cylinder. The in-cylinder velocity field distribution is layered, and the gas flow near the solid wall has a high velocity and gradually spreads out. Irregular small-scale vortices are formed in the local high-pressure zone C below the outlet valve, as shown in Figure 8e, because of the decrease in overall vortex velocity. The overall velocity of gas flow around the intake valve increases again with the decrease in inlet valve opening degree at the end of intake process. Furthermore, vortices V_1 and V_2 enter the dissipation stage as the overall distributions of velocity and pressure become uniform in the cylinder. Irregular small-scale vortices are formed below the inlet valve (*i.e.*, the narrow channel between the inlet valve and the cylinder), as shown in Figure 8f.

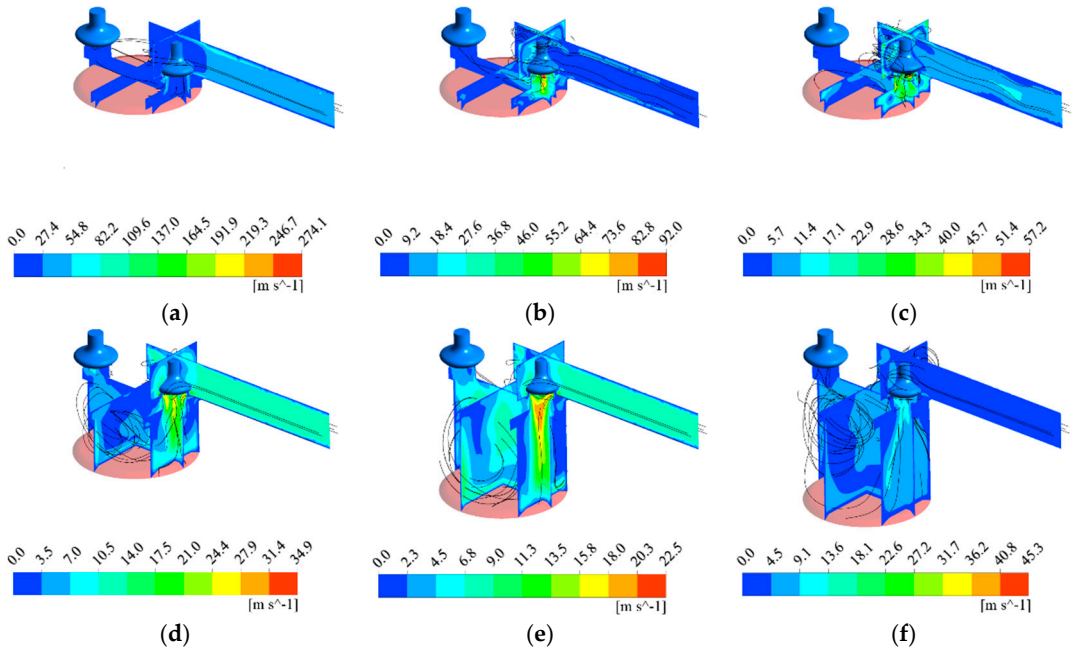

Figure 8. Velocity distribution and streamlines during the intake process: (**a**) θ = 2°; (**b**) θ = 10°; (**c**) θ = 14°; (**d**) θ = 45°; (**e**) θ = 75°; (**f**) θ = 88°.

Vortices form in the cylinder, and they change with inlet valve opening degree and piston displacement during the intake process. Vortex flow converts pressure energy and kinetic energy into thermodynamic energy for the working fluid, which weakens the power capacity of the working fluid within a certain period [40,41]. Several practical approaches should be adopted to adjust the intake flow and reduce the energy losses caused by large-scale vortex flow, and thus, improve the energy conversion efficiency of the FPE. Examples of such approaches include optimizing the inner structure of the cylinder, modifying inlet valve shape and size, and reducing the length of the inlet port.

Figure 9 shows the gas velocity distribution during the exhaust process at different cam plate rotational angles after the beginning of the curved surface for lifting the inlet valve (ranges from 185° to 275°). Compared with that in the intake process, flow velocity is lower during the exhaust process. Gas flow with high velocity mainly occurs in the flow area between the outlet valve and the outlet valve seat. For in-cylinder gas flow, compared with exhaust velocity, velocity of vortex flow can be ignored.

The aforementioned work can provide a theoretical foundation to improve and optimize the conceptual design of next-generation FPEs.

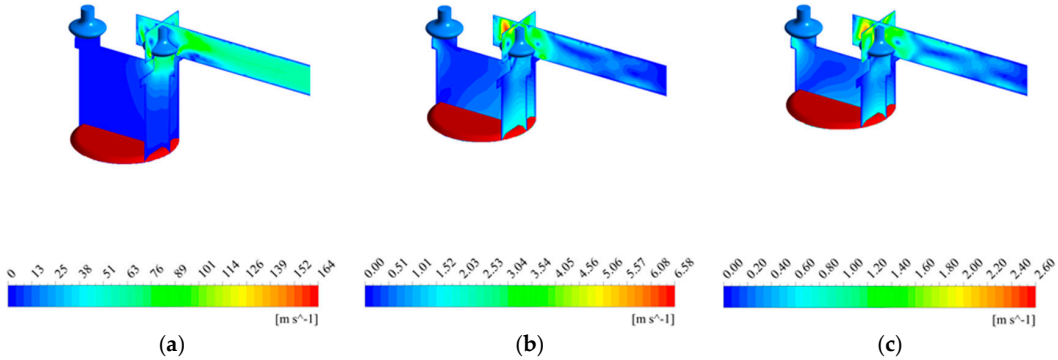

Figure 9. Velocity distribution during the exhaust process: (**a**) θ = 185°; (**b**) θ = 245°; (**c**) θ = 275°.

3.2. *Analysis of the Actual Working Process of the Free Piston Expander*

Figure 10 shows the variation of in-cylinder pressure and piston displacement at various working frequencies of FPE A when the intake pressure is 0.2 MPa and the intake temperature is 300 K. As shown in Figure 10, the actual stroke length of the piston decreases with the increase in working frequency. When working frequency is low, the piston-mover group moves rapidly from TDC to BDC and reaches BDC during the intake process because intake time is long and the electromagnetic force is insufficiently large. Then, the piston-mover group stops moving for a certain period until the exhaust stroke (process) begins. No effective expansion process actually occurs in the cylinder of the FPE, which results in an extremely low energy conversion efficiency. In addition, collision between the piston and the cylinder head may occur in the other FPE. This becomes the largest damage risk for such a system [42]. Two possible solutions are proposed to solve the aforementioned problem. On the one hand, the working frequency of the FPE should be increased (higher than 2.5 Hz). On the other hand, the LG should be efficiently matched with the FPEs, and a reasonable valve timing and valve duration should be determined.

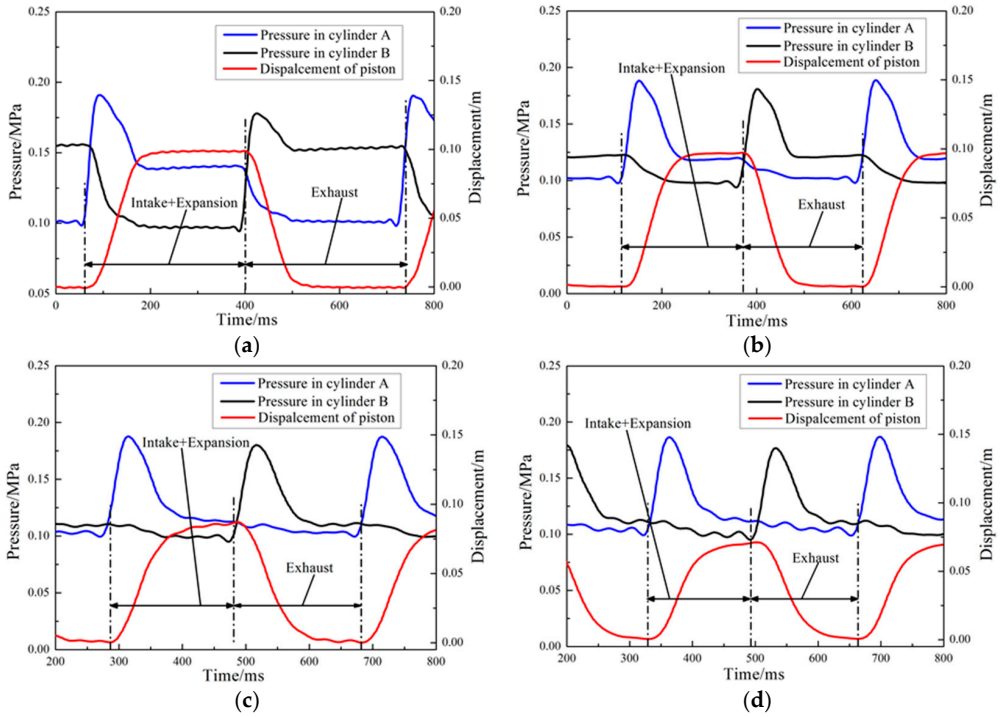

Figure 10. Variation of in-cylinder pressure and piston displacement of the FPE A: (**a**) 1.5 Hz; (**b**) 2 Hz; (**c**) 2.5 Hz; (**d**) 3 Hz.

Furthermore, a natural frequency of operation exists if the piston working frequency is increased from 3 Hz to a different value that eliminates the piston dwell time at top or bottom dead center. In reference [42], a simulation model on the FPLA (which is similar to the FPE-LG except for combustion process) is formed in a MATLAB/Simulink environment. According to the theoretical analysis, the system can be equivalent to a linear single-degree-of-freedom discrete system with variable damping and stiffness. It can be considered that the natural frequency is only decided by the mass and the equivalent stiffness. It can be written as:

$$f_0 = \frac{1}{2\pi}\sqrt{k/m} = \frac{1}{\pi}\sqrt{\frac{1}{-\gamma+1}P_0 L^{-1} A(\frac{1}{2^\gamma}-1)m^{-1}} \quad (1)$$

where P_0 is the cylinder pressure at the equilibrium position, L is the oscillation amplitude, γ is the polytropic exponent, A is the piston cross sectional area. For the FPLA system, the natural frequency has some relationship with P_0 and L. They are variables varying with the external excitation. All the variables can be set to the proper ranges. This means that the FPLA has a compression ratio range which can cover the full working range of this engine in the studied case.

As mentioned in reference [42], the piston motion frequency depends on intake pressure, moving mass, and loads, *etc.* It is not constrained. Thus, each combination of these parameters decides one working condition. Theoretically these parameters can be gradually adjusted to achieve certain frequency. However, at present, some mechanical wears exist between the cam plate and the valve sliders. Meanwhile, the value of external load resistance is small during the tests. Hence, from the view of safety, the working frequency (more than 3 Hz) has not been continued increasing in preliminary tests. This problem will be tried to resolve and the natural frequency will be estimated in the future work based on the method in reference [42] and more experimental studies.

3.3. Indicated Efficiency of the Free Piston Expander

In this research, the indicated efficiency of FPE A is analyzed based on the *p*–*V* indicator diagram of FPE A. The in-cylinder pressure variation of FPE A, as well as the comparison between the ideal working process and actual working process, is shown in Figure 11 when the working frequency is 3 Hz, the intake pressure is 0.2 MPa, and the load resistance is 5 Ω.

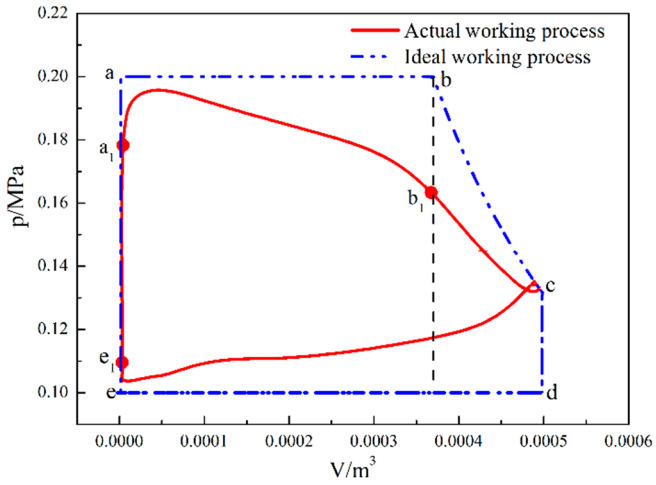

Figure 11. *p*–*V* indicator diagram of the FPE A.

In Figure 11, Process e_1-a_1-b_1 is the actual intake process, Process e-a-b is the ideal intake process, Process b_1-c is the actual expansion process, Process b-c is the ideal expansion process, Process c-e_1 is the actual exhaust process, and Process c-d-e is the ideal exhaust process. We define the

indicated efficiency of the FPE as the ratio of the area surrounded by the curves representing the actual working process to the area surrounded by the curves representing the ideal working process. Thereby, according to test data shown in Figure 11, the indicated efficiency of FPE A is 66.2%. Based on the *p*–*V* indicator diagram of the FPE, we define the indicated energy loss ratio of the FPE as the ratio of the area between the curves representing the actual working process and the curves representing the ideal working process to the area surrounded by the curves representing the ideal working process. According to the test data shown in Figure 11, the total energy loss ratio of FPE A is 33.8%. The energy loss ratio that corresponds to intake process is 12.9% (*i.e.*, the ratio of the area between the curves representing the actual intake process and the curves representing the ideal intake process to the area surrounded by the curves representing the ideal working process), the energy loss ratio that corresponds to the expansion process is 4.9% (*i.e.*, the ratio of the area between the curves representing the actual expansion process and the curves representing the ideal expansion process to the area surrounded by the curves representing the ideal working process), and the energy loss ratio that corresponds to the exhaust process is 16% (*i.e.*, the ratio of the area between the curves representing the actual exhaust process and the curves representing the ideal exhaust process to the area surrounded by the curves representing the ideal working process).

Figure 12a shows the *p*–*V* indicator diagram for FPE A at different intake pressures when the working frequency, the load resistance, and the intake temperature are 2 Hz, 5 Ω, and 300 K, respectively. We define variable *V* on the X-axis as sweep volume of the expander (*i.e.*, total cylinder volume less clearance volume). The clearance volume includes two parts: the first part is formed with the cylinder head, the cylinder block, and the piston when the piston reached TDC; and the second part is formed with the cylinder cover, the cylinder block, and the piston when the piston reached BDC. With the increase of intake pressure, the power output and the actual piston stroke length both increase. The difference between the intake pressure and the peak value of the in-cylinder pressure also increases. As shown in Figure 12b, we define variable P_{in} on the X-axis as the intake pressure of the expander. The indicated efficiency of FPE A decreases with the increase in intake pressure. The energy loss ratios that correspond to the intake and exhaust processes evidently increase.

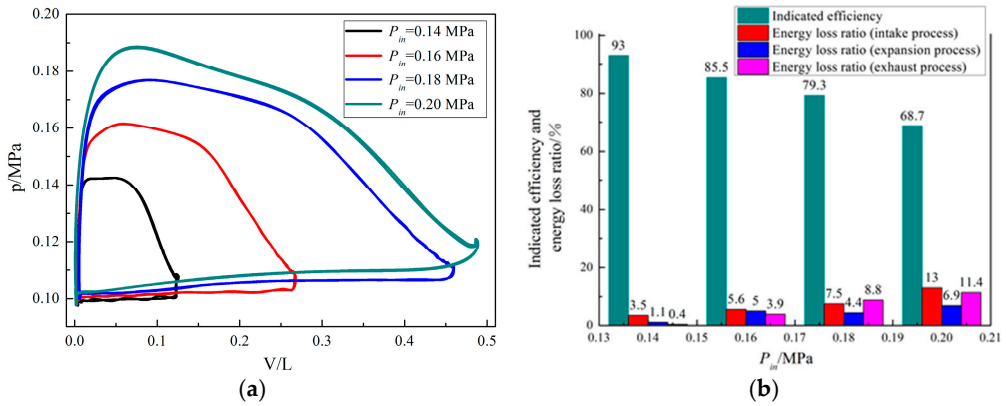

Figure 12. *p*–*V* diagram and indicated efficiency for different intake pressures: (**a**) *p*–*V* diagram for different intake pressures; (**b**) indicated efficiency and energy losses.

3.4. Electric Power Output of Free Piston Expander-Linear Generator

The variation tendency of the electric power output with the intake pressure is shown in Figure 13 when the load resistance and the working frequency of the FPE-LG are 5 Ω and 3 Hz, respectively. As can be seen in Figure 13, the electric power output of the FPE-LG generally increases substantially with the improvement of the intake pressure, but the increasing extent differs. The variation of the electric power output is small at low working frequencies, whereas the increase in the electric power

output is comparatively obvious at high working frequencies. The maximal electric power output of the FPE-LG can reach 22.7 W when the intake pressure is 0.2 MPa.

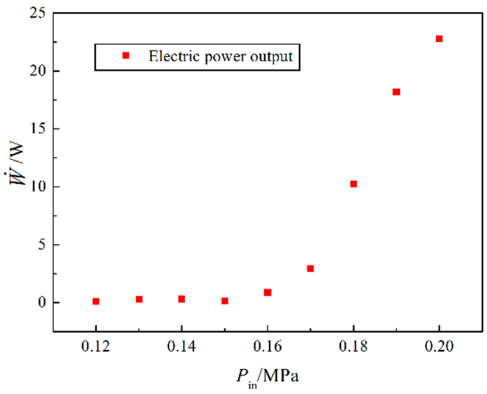

Figure 13. Electric power output of FPE-LG.

4. Conclusions

Based on this initial work, the FPE-LG shows promising potential for continued development as a simple and efficient thermo-electric conversion unit. This research focuses on the development of the FPE-LG, as well as on the conceptual design and 3D numerical simulation of the FPE. In addition, several preliminary experiments based on an air test rig have been conducted. The main research findings can be summarized as follows:

(1) The working principle of the FPE-LG is proven feasible through the air test rig. However, further test of the FPE-LG in a small-scale ORC system should be performed in the future;
(2) The energy-conversion efficiency of the expander is obviously affected by the intake parameters. The indicated efficiency of the FPE can reach 66.2% and the maximal electric power output of the FPE-LG can reach 22.7 W when the working frequency is 3 Hz and the intake pressure is 0.2 MPa;
(3) Two large-scale vortices are formed during the intake process. To improve the energy conversion efficiency of the FPE, several practical approaches should be adopted to adjust the intake flow and to reduce the energy losses caused by large-scale vortex flow.

Several conclusions may be drawn from this design study. First, a linear generator with a larger thrust force are desirable to increase output power of FPE-LG and avoid collisions between the piston and the cylinder head at low working frequencies. Second, the mechanical strength of related parts in the valve train needs to be improved to further increase the working frequency. Meanwhile, the cam plate intake duration needs to be decreased, whereas the duration of the expansion process needs to be increased. Third, in its final form, installation space is a premium consideration for the FPE-LG. This unit will be designed to be modular, and thus, the number of these units can be flexibly adjusted according to the output power requirement for a wide variety of small-scale vehicle ORC systems.

These results are greatly beneficial to next generation FPE-LG development. More experimental testing of the optimized FPE-LG performance will be conducted using the guidelines established in this work as a foundation. Future CFD simulation with organic working fluid will be conducted in an attempt to further reveal the in-cylinder flow characteristics.

Acknowledgments: This work was sponsored by the Beijing Natural Science Foundation Program (Grant No. 3152005), the Scientific Research Key Program of Beijing Municipal Commission of Education (Grant No. KZ201410005003), the National Natural Science Foundation of China (Grant No. 51376011), the National Basic Research Program of China (973 Program) (Grant No. 2013CB228306), the Project of Fourteenth Scientific Research Foundation for Graduate Students in Beijing University of Technology (Grant No. ykj-2015-12128), and Research Fund for Doctoral Program of Higher Education of China (Grant No. 3C005015201301). The authors would like to thank the reviewers for their valuable comments on this research.

Author Contributions: Gaosheng Li wrote the main body of the paper. Hongguang Zhang and Fubin Yang revised the paper. Songsong Song, Ying Chang, and Fei Yu performed the simulations. Jingfu Wang and Baofeng Yao performed the experiments. All authors read and approved the manuscript.

Conflicts of Interest: The authors declare no conflict of interests.

Nomenclature

p	in-cylinder pressure (MPa)
P_{in}	intake pressure (MPa)
V	sweep volume (L)
θ	cam plate rotational angles after the beginning of the curved surface for lifting up inlet valve (degree)
$\dot{W}$	electric power output (W)
P_0	cylinder pressure at the equilibrium position (MPa)
L	oscillation amplitude (m)
γ	polytropic exponent
A	piston cross sectional area (m^2)
m	moving mass (kg)
f_0	natural frequency (Hz)
k	the equivalent stiffness (N/m)

Acronyms

FPE	free piston expander
LG	linear generator
IC	internal combustion
TDC	top dead center
BDC	bottom dead center
WHR	waste heat recovery
ORC	organic Rankine cycle
CFD	computational fluid dynamic

References

1. Aghaali, H.; Ångström, H.E. A review of turbocompounding as a waste heat recovery system for internal combustion engines. *Renew. Sustain. Energy Rev.* **2015**, *49*, 813–824. [CrossRef]
2. Yu, G.P.; Shu, G.Q.; Tian, H.; Wei, H.Q.; Liu, L.N. Simulation and thermodynamic analysis of a bottoming organic Rankine cycle (ORC) of diesel engine (DE). *Energy* **2013**, *51*, 281–290. [CrossRef]
3. Saidur, R.; Rezaei, M.; Muzammil, W.K.; Hassan, M.H.; Paria, S.; Hasanuzzaman, M. Technologies to recover exhaust heat from internal combustion engines. *Renew. Sustain. Energy Rev.* **2012**, *16*, 5649–5659. [CrossRef]
4. Sprouse, C.; Depcik, C. Review of organic Rankine cycles for internal combustion engine exhaust waste heat recovery. *Appl. Therm. Eng.* **2013**, *51*, 711–722. [CrossRef]
5. Song, J.; Gu, C.W. Parametric analysis of a dual loop Organic Rankine Cycle (ORC) system for engine waste heat recovery. *Energy Convers. Manag.* **2015**, *105*, 995–1005. [CrossRef]
6. Quoilin, S.; Aumann, R.; Grill, A.; Schuster, A.; Lemort, V.; Spliethoff, H. Dynamic modeling and optimal control strategy of waste heat recovery Organic Rankine Cycles. *Appl. Energy* **2011**, *88*, 2183–2190. [CrossRef]
7. Yang, F.B.; Zhang, H.G.; Bei, C.; Song, S.S.; Wang, E.H. Parametric optimization and performance analysis of ORC (organic Rankine cycle) for diesel engine waste heat recovery with a fin-and-tube evaporator. *Energy* **2015**, *91*, 128–141. [CrossRef]
8. Kang, S.H. Design and preliminary tests of ORC (organic Rankine cycle) with two-stage radial turbine. *Energy* **2016**, *96*, 142–154. [CrossRef]
9. Horst, T.A.; Tegethoff, W.; Eilts, P.; Koehler, J. Prediction of dynamic Rankine Cycle waste heat recovery performance and fuel saving potential in passenger car applications considering interactions with vehicles' energy management. *Energy Convers. Manag.* **2014**, *78*, 438–451. [CrossRef]

10. Tang, H.; Wu, H.G.; Wang, X.L.; Xing, Z.W. Performance study of a twin-screw expander used in a geothermal organic Rankine cycle power generator. *Energy* **2015**, *90*, 631–642. [CrossRef]
11. Wu, Y.T.; Lei, B.; Ma, C.F.; Zhao, L.; Wang, J.F.; Guo, H.; Lu, Y.W. Study on the Characteristics of Expander Power Output Used for Offsetting Pumping Work Consumption in Organic Rankine Cycles. *Energies* **2014**, *7*, 4957–4971. [CrossRef]
12. Quoilin, S. Sustainable energy conversion through the use of organic Rankine cycles for waste heat recovery and solar applications. Ph.D. Thesis, University of Liège, Wallonia, Belgium, 2011.
13. Antonelli, M.; Baccioli, A.; Francesconi, M.; Desideri, U.; Martorano, L. Operating maps of a rotary engine used as an expander for micro-generation with various working fluids. *Appl. Energy* **2014**, *113*, 742–750. [CrossRef]
14. Ziviani, D.; Beyene, A.; Venturini, M. Advances and challenges in ORC systems modeling for low grade thermal energy recovery. *Appl. Energy* **2014**, *121*, 79–95. [CrossRef]
15. Qiu, G.Q.; Liu, H.; Riffat, S. Expanders for micro-CHP systems with organic Rankine cycle. *Appl. Therm. Eng.* **2011**, *31*, 3301–3307. [CrossRef]
16. Muhammad, I.; Muhammad, U.; Park, B.S.; Lee, D.H. Volumetric expanders for low grade heat and waste heat recovery applications. *Renew. Sustain. Energy Rev.* **2016**, *57*, 1090–1109.
17. Bao, J.J.; Zhao, L. A review of working fluid and expander selections for organic Rankine cycle. *Renew. Sustain. Energy Rev.* **2013**, *24*, 325–342. [CrossRef]
18. Quoilin, S.; Van Den Broek, M.; Declaye, S.; Dewallef, P.; Lemort, V. Technoeconomic survey of Organic Rankine Cycle (ORC) systems. *Renew. Sustain. Energy Rev.* **2013**, *22*, 168–186. [CrossRef]
19. Young, M.K.; Dong, G.S.; Chang, G.K. Optimization of Design Pressure Ratio of Positive Displacement Expander for Vehicle Engine Waste Heat Recovery. *Energies* **2014**, *7*, 6105–6117.
20. Declaye, S.; Quoilin, S.; Guillaume, L.; Lemort, V. Experimental study on an open-drive scroll expander integrated into an ORC (Organic Rankine Cycle) system with R245fa as working fluid. *Energy* **2013**, *55*, 173–183. [CrossRef]
21. Clemente, S.; Micheli, D.; Reini, M.; Taccani, R. Energy efficiency analysis of organic Rankine cycles with scroll expanders for cogenerative applications. *Appl. Energy* **2012**, *97*, 792–801. [CrossRef]
22. Lemort, V.; Quoilin, S.; Cuevas, C.; Lebrun, J. Testing and modeling a scroll expander integrated into an organic Rankine cycle. *Appl. Therm. Eng.* **2009**, *29*, 3094–3102. [CrossRef]
23. Gao, W.Z.; Zhai, J.M.; Li, G.H.; Bian, Q.; Feng, L.M. Performance evaluation and experiment system for waste heat recovery of diesel engine. *Energy* **2013**, *55*, 226–235.
24. Glavatskaya, Y.; Podevin, P.; Lemort, V.; Shonda, O.; Descombes, G. Reciprocating Expander for an Exhaust Heat Recovery Rankine Cycle for a Passenger Car Application. *Energies* **2012**, *5*, 1751–1765. [CrossRef]
25. Chiong, M.; Rajoo, S.; Romagnoli, A. Nozzle Steam Piston Expander for Engine Exhaust Energy Recovery. *SAE Tech. Pap.* **2015**. [CrossRef]
26. Badami, M.; Mura, M. Preliminary design and controlling strategies of a small-scale wood waste Rankine Cycle (RC) with a reciprocating steam engine (SE). *Energy* **2009**, *34*, 1315–1324. [CrossRef]
27. Zhang, B.; Peng, X.; He, Z.; Xing, Z.; Shu, P. Development of a double acting free piston expander for power recovery in transcritical CO_2 cycle. *Appl. Therm. Eng.* **2007**, *27*, 1629–1636. [CrossRef]
28. Han, Y.Q.; Kang, J.J.; Zhang, G.P.; Liu, Z.C.; Tian, J.; Chai, J.H. Performance evaluation of free piston compressor coupling organic Rankine cycle under different operating conditions. *Energy Convers. Manag.* **2014**, *86*, 340–348. [CrossRef]
29. Han, Y.Q.; Kang, J.J.; Wang, X.F.; Liu, Z.C.; Tian, J.; Wang, Y.Q. Modelling and simulation analysis of an ORC-FPC waste heat recovery system for the stationary CNG-fuelled compressor. *Appl. Therm. Eng.* **2015**, *87*, 481–490. [CrossRef]
30. Weiss, L.W. Study of a MEMS-Based free piston expander for energy sustainability. *J. Mech. Des.* **2010**, *132*, 1–8. [CrossRef]
31. Champagne, C.; Weiss, L. Performance analysis of a miniature free piston expander for waste heat energy harvesting. *Energy Convers. Manag.* **2013**, *76*, 883–892. [CrossRef]
32. Nickl, J.; Will, G.; Quack, H.; Kraus, W.E. Integration of a three-stage expander into a CO_2 refrigeration system. *Int. J. Refrig.* **2005**, *28*, 1219–1224. [CrossRef]
33. Li, Q.F.; Xiao, J.; Huang, Z. Simulation of a two-stroke free-piston engine for electrical power generation. *Energy Fuels* **2008**, *22*, 3443–3449. [CrossRef]

34. Feng, H.H.; Song, Y.; Zuo, Z.X.; Shang, J.; Wang, Y.D.; Roskilly, A.P. Stable Operation and Electricity Generating Characteristics of a Single-Cylinder Free Piston Engine Linear Generator: Simulation and Experiments. *Energies* **2015**, *8*, 765–785. [CrossRef]
35. Yuan, C.H. Research on Performance Characteristics and Design Technology of Free-piston Diesel Engine for Linear Generator. Ph.D. Thesis, Beijing Institute of Technology, Beijing, China, 2014.
36. Jiang, Y.T.; Ma, Y.T.; Fu, L.; Li, M.X. Some design features of CO_2 two-rolling piston expander. *Energy* **2013**, *55*, 916–924. [CrossRef]
37. Baek, J.S.; Groll, E.A.; Lawless, P.B. Piston-cylinder work producing expansion device in a transcritical carbon dioxide cycle. Part I: Experimental investigation. *Int. J. Refrig.* **2005**, *28*, 141–151. [CrossRef]
38. Wang, W.; Wu, Y.T.; Ma, C.F.; Liu, L.D.; Yu, J. Preliminary experimental study of single screw expander prototype. *Appl. Therm. Eng.* **2011**, *31*, 3684–3688. [CrossRef]
39. Turbulence. *ANSYS FLUENT Release 14.5 Theroy Guide*; ANSYS Inc.: Cecil Township, PA, USA, 2012; pp. 51–54.
40. Wei, M.S.; Song, P.P.; Zhao, B.; Shi, L.; Wang, Z.X.; Ma, C.C. Unsteady flow in the suction process of a scroll expander for an ORC waste heat recovery system. *Appl. Therm. Eng.* **2015**, *78*, 460–470. [CrossRef]
41. Song, P.P.; Wei, M.S.; Liu, Z.; Zhao, B. Effects of suction port arrangements on a scroll expander for a small scale ORC system based on CFD approach. *Appl. Energy* **2015**, *150*, 274–285. [CrossRef]
42. Xiao, J.; Li, Q.F.; Huang, Z. Motion characteristic of a free piston linear engine. *Appl. Energy* **2010**, *87*, 1288–1294. [CrossRef]